XANES and XPS study of electronic structure of Ti-enriched Nd−Fe−B ribbons

V. Bilovol [a,*], S. Ferrari [a], D. Derewnicka [b], F.D. Saccone [a]

[a] Laboratorio de Sólidos Amorfos, INTECIN-CONICET, Facultad de Ingeniería, Universidad de Buenos Aires, Buenos Aires C1063ACV, Argentina
[b] Institute of Precision Mechanics, Duchnicka 3, 01-796 Warsaw, Poland

HIGHLIGHTS

- Rapidly quenched ribbons of Nd−Fe−B−Ti alloys were prepared by melt-spinning.
- Ti addition promotes modifications of the electronic structure of Fe sub-band.
- Evidences of acceptor nature of Ti and Fe in Nd−Fe−B−Ti alloys are present.
- Nd, Fe, Ti on the surface of the ribbons were found in both metallic and oxidized state.

ARTICLE INFO

ABSTRACT

Electronic structure of rapidly quenched ribbons of nominal composition $Nd_yFe_{(86−y−x)}B_{14}Ti_x$ ($x = 0, 2, 4$; $y = 7, 8$ at.%) was studied by X-ray absorption (Fe and Ti K-edge) and X-ray photoelectron spectroscopy. It was found by XANES that Ti addition promotes modifications of the electronic structure of Fe sub-band. From the analysis of differences in the pre-edges structure areas, coming from variations in the $3d$ density of states near the Fermi level, the evidences of acceptor nature of Ti and Fe atoms in NdFeB alloys are present. Using photoelectron spectroscopy, we found that neodymium, iron and titanium are in both, metallic and oxidized, states on the surface of the ribbons. A higher Ti^0 content (at high vacuum) is characteristic of the annealed samples. The presence of oxidized titanium states was corroborated by XANES.

© 2014 Elsevier B.V. All rights reserved.

1. Introduction

NdFeB-based alloys, one of the main known materials for permanent magnets industry up to now, are still the target of broad scientific and engineering attention [1–3]. The reason of such interest is to seek improved magnetic properties of these magnets: high coercive field and maximum energy product. One of the successful solutions to this task, in particular for nanostructured Nd−Fe−B alloys, is adding other chemical elements which help to control the grain growth during annealing. For these alloys (with low Nd content) the mechanism of their crystallization becomes modified when they are enriched with Ti, Nb and/or Mo, creating an optimized nanostructure that induces better magnetic properties of these materials [4,5]. In particular, it has been suggested that titanium addition retards the nucleation and growth of metallic

iron, favoring crystallization of magnetically hard $Nd_2Fe_{14}B$ phase [6]. It was shown that among $Nd_yFe_{(86−y−x)}B_{14}Ti_x$ ($x = 0, 2, 4$; $y = 7, 8$ at.%) ribbons, the best magnetic properties were found for 8 at.% of Nd and 4 at.% of Ti content (a higher energy product and a higher coercive field) [7].

There are extensive studies of Nd−Fe−B alloys by means of XRD, SEM/TEM, Mössbauer spectroscopy and magnetic measurements [8–12]. On the other hand, poor attention was paid to study such materials by synchrotron radiation techniques [13]. Synchrotron radiation is a powerful tool that helps to elucidate many structural and electronic modifications that can occur at the neighborhood of atoms after material synthesis. One of these tools is the X-ray absorption spectroscopy technique that consists of X-ray Absorption Near Edge Spectroscopy (XANES) and Extended X-ray Absorption Fine Structure (EXAFS). XANES is associated with the excitation process of a core electron to unoccupied bounded states and provides information on the electronic state of the X-ray absorbing atom and on its surrounding local structure, making this technique very useful for amorphous and/or highly dispersed phases. Thus,

* Corresponding author.
    E-mail address: vbilovol@fi.uba.ar (V. Bilovol).

XANES is very suitable tool for studying electronic structure. It is of particular importance in the case of absorption measurements at K-edge of magnetic elements such as Fe, because of involved 3d bands whose electrons contribute to magnetic moments that is reflected in magnetic response of material.

X-ray photoelectron spectroscopy (XPS) is a versatile surface analysis technique that can be used for compositional and chemical states analysis. By irradiating a sample with monoenergetic soft X-rays, the surface region atoms interact with them by photoelectric effect, causing electrons (with a characteristic binding energy) to be emitted. XPS is routinely used to examine the electronic structure of surfaces of materials in the solid state.

In this work we focused our attention on electronic structure of as-quenched and thermally annealed Nd$_y$Fe$_{(86-y-x)}$B$_{14}$Ti$_x$ (x = 0, 2, 4; y = 7, 8 at.%) alloys with more emphasis on the Fe and Ti electronic states. The outline of the Results and discussion chapter is as it follows. At first, we employ XAS technique: Ti K-edge XANES spectra measured in fluorescence mode (Section 3.1), next we analyze the results from Fe K-edge XANES in transmission mode (Section 3.2). We compare as-quenched samples (AQ) with thermally treated (TT) in Section 3.3. Fourier transformations of the oscillating part of the spectra of TT samples (Fe K-edge) are briefly treated in Section 3.4 as well as XRD results. Section 3.5 is dedicated to XPS study of survey spectra (Section 3.5.1) and to titanium 2p electrons (Section 3.5.2).

2. Experimental

The starting ingots were prepared by arc melting of pure elements in argon atmosphere. The ribbons were prepared by rapid solidification of molten alloy by melt-spinning with the roll speed of 20 m s^{-1}. Ribbons were sealed in quartz ampoules in protective atmosphere of argon. Then the overquenched ribbons were annealed at 973 K for 20 min. The thickness of the ribbons was about 20 μm. The samples were labeled as NdyTix_YY (y = 7, 8; x = 0, 2, 4, YY: AQ, TT).

The samples for XAS experiments were prepared in the form of 5 mm-diameter pellets using standard pressure procedure. Boron nitride powder was used mixed with previously sieved 5μ-mesh powder of NdFeBTi alloy (it was slightly milled previously). The mass of the powders was estimated to optimize the absorption jump.

All spectroscopic measurements were performed at Laboratorio Nacional de Luz Sincrotron, Campinas, Brazil. The XAFS experiments (X-ray absorption near-edge structure) were carried out using the D04B-XAS1 beamline at Fe K-edge (the D08B-XAS2 beamline at Ti K-edge). The Fe K-edge spectra were collected in transmission mode of samples in powder form (the Ti K-edge spectra were collected in fluorescence mode at room temperature) using a Si(1 1 1) single channel-cut crystal monochromator (double crystal at XAS2) at 15 K with a slit aperture of 0.5 mm, to obtain an energy resolution of about 1 eV. The detectors were three ion chambers filled with air at atmospheric pressure. The energy calibration was obtained by simultaneous absorption measurements on the Fe (or Ti) metal sample positioned between the second and the third ionization chamber. X-ray absorption data were analyzed by using standards procedures: a linear background was fitted at the pre-edge region and then subtracted from the entire spectrum; the jump of the spectrum was normalized to unity with the post-edge asymptotic value by using a quadratic fit. All these procedures as well as the EXAFS analysis were performed using IFEFFIT package (version 1.2.11). The XAFS signal $\chi(k)$, covering a k range from 2 to 14 Å^{-1}, was Fourier transformed to R space using k weightings of 2 and a Hanning window with window sills dk equal to 2. The ARTEMIS option for simultaneous fits with all three k

weightings 1, 2, and 3 was used. The reference paths were calculated using the FEFF7 algorithm. The pre-peak areas of XANES signal were calculated using freely available XANES dactyloscope software (XANDA, version 2012/04).

XPS was performed using a PHOIBOS150 hemispherical spectrometer from SPECS (Berlin, Germany), using the HSA3500 high-voltage power supply. The detection was achieved using the constant analyzer energy mode. The XPS had a monochromatic Al Kα ($h\nu$ = 1486.6 eV) source and a nine-channel electron multiplier detector. The samples in ribbon form were supported on copper double-sided tape fixed on the XPS sample holder. Survey scans were acquired with a pass-energy of 40 eV, 1.0 eV step-size, while narrow scans were acquired with a pass-energy of 40 eV, 0.2 eV step-size. The instrument work function was calibrated to give an Au 4f$_{7/2}$ metallic gold binding energy (BE) of 83.95 eV. Spectra were analyzed with CasaXPS software (version 2.3.16). Gaussian (70%)–Lorentzian (30%) profiles were used for each component, except for Ti metallic core lines, where asymmetry was defined in the form of LA(α,β,m) where α and β define the spread of the tail on either side of the Lorentzian component. The parameter m specifies the width of the Gaussian used to convolute the Lorentzian curve. A standard Shirley background is used for all reference sample spectra.

X-ray diffraction patterns were measured with Rigaku (model D/max 22) diffractometer (equipped with a vertical goniometer and using Bragg–Brentano geometry) with Cu-Kα radiation running in the 2θ = 30°–80° range, step 0.05° with a velocity of 0.4° min^{-1}. The obtained spectra were analyzed by Rietveld refinement using the Maud [14] program.

3. Results and discussion

3.1. Ti K-edge XANES

Region XANES of the metallic Ti K-edge, measured as a reference (Figs. 1 and 3,,), has two pre-edge features: a sharp pre-peak and a shoulder. It is established that in the 3d elements the pre-peak at the edge of the spectra can be identified with the large 3d density of states [15]. Pre-edge peak is assigned as quadrupole transitions from the 1s core state to the empty 3d states. In case the inversion symmetry of the transition metal is broken, the pre-edge gains additional intensity due to the local 3d 4p wavefunction mixing, effectively allowing dipole transitions to the 4p character of the 3d-band [16]. The interpretation of the shoulder is more controversial. For instance, Glen and Dodd claimed that it is due to *1s-to-4p* monopole transition [17], although Grunes questioned it because this transition is too weak to be observed [18].

As it can be seen, the XANES signal of Ti foil indicates that Ti coordination in the metal is different from that in the alloys. It means that Ti in Nd–Fe–B alloys does not have the same neighbor coordination which Ti atom has in Ti foil. By this reason, Ti cluster formation can be discarded within the sensitivity threshold of the technique. In the spectra of the samples a pre-peak is not clearly visible (there is no sharp peak). It is associated with the corresponding filling of the 3d band [15]. We assume the area of pre-edge structure is due to the occupancy of the available 3d states. We evaluated the total area under pre-edge structures since there was no way to isolate each individual contribution (pre-peak and shoulder are very close to each other).

In Fig. 1, we show a comparison of XANES signals with fixed Nd content while Ti content is varied (x = 2, 4 at.%). Fig. 1a) corresponds to AQ samples with y = 7 at.%: we compare the signal of the samples with the reference one, it is seen that the pre-edge area decreases (Fig. 2a) while the intensity of the main line increases. The former feature corresponds to the lower empty density state (EDS) in the Ti 3d sub-band, while the latter means that the lower
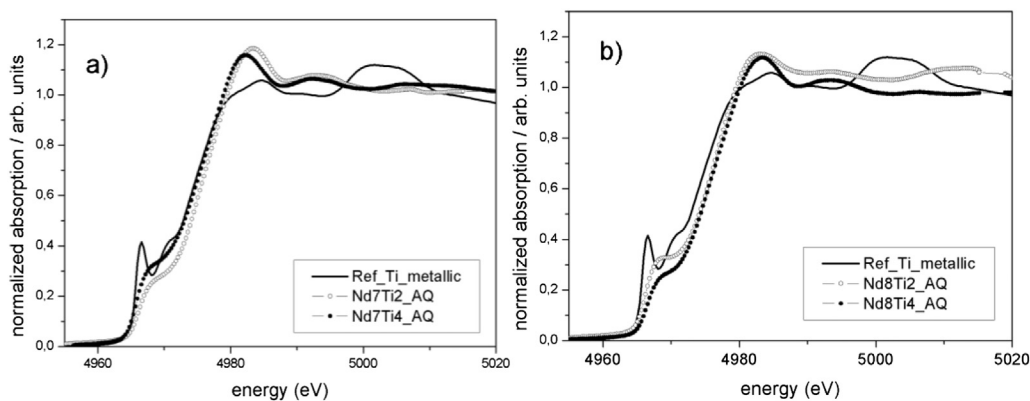
Fig. 1. Ti K-edge XANES signal of metallic Ti and AQ alloys with varied Ti content ($x = 2,4$ at.%) and varied Nd content a) $y = 7$ at.% and b) $y = 8$ at.%.

EDS is coming from a minor number of $1s \rightarrow 4p$ transitions. Both features in the spectra are also observed in Fig. 1b) for AQ samples with higher Nd concentration (8 at.%). An interesting difference between the spectra with fixed Nd concentration consists in the opposite tendencies in orbital filling: for higher Nd content, the orbital occupancy increases as Ti content increases from 2 to 4 at.%; while for lower Nd content, the orbital occupancy decreases as Ti content increases from 2 to 4 at.%.

On the other hand, the common feature of these spectra is a main line shift in the ($1s \rightarrow 4p$ dipolar transition) position respect to metallic Ti one. This fact indicates an existence of partially oxidized titanium states. We note that all spectra of AQ alloys are slightly shifted to higher energy values. It is worth emphasizing that the main line position is very sensitive to the changes in the oxidation state so that even a presence of low amount of oxidized probe atom (titanium, in this case) can influence the line position. All spectral features mentioned above were typical and observed in Ti K-edge XANES spectra of TT alloys.

3.2. Fe K-edge XANES

In Fig. 3a), the XANES spectra at Fe K-edge are shown for AQ ribbons with $y = 7$ at.% and Ti concentration of 0, 2 and 4 at.%. It is seen that Ti addition influences Fe 3d empty density states. When Ti concentration reaches 2–4 at.%, 3d empty density states in Fe sub-band is higher. The main line intensity diminishes strongly when Ti is added, indicating a reduced number of $1s$-$4p$ transitions.

On the contrary, when Nd concentration is 8 at.%, the tendency of EDS of 3d levels of Fe is different (Fig. 3b): when Ti concentration increases from 0 up to 4%, the EDS of 3d levels of iron diminishes (in a contrast with AQ samples with 7 at.% of neodymium, for which the filling levels of 3d states goes in the opposite tendency). On the other hand, the EDS of 4p of iron is increased notoriously in alloy containing 4 at.% of titanium, as it is concluded from its higher main line intensity. A higher intensity of pre-edge structure does not necessary involve a larger area below it. This conclusion could lead to an error when visual comparisons are done with the data shown in Fig. 2. The example of such situation is shown in Fig. 3c), where one sees that the larger area under the pre-edge structure (Nd8Ti4_AQ) does not correspond to the spectrum with higher pre-edge intensity (Nd8Ti2_AQ). It is important to underline that pre-edge structure calculation is critically dependent on the spectra normalization. Fig. 3d) shows the normalized spectra of the samples with $y = 8$ at.% at large scale.

When pre-edge structure areas were calculated (Fig. 2b), they resulted to be smaller as compared to metallic Fe, indicating a diminishing of 3d empty density states near the Fermi level (in similarity with Ti 3d states). In the case of Fe atoms, this could be particularly important because more electrons would be able to contribute to the total magnetic moment of the Fe atoms. On the other hand, the observed changes in the electronic structure are not the only and/or direct cause of the magnetic properties of the alloys under study.

In Fig. 4, the comparison of the spectra with varied Nd content is given. For AQ samples without Ti (Fig. 4a) we observe a reduction of 3d EDS and an increase of 4p EDS of Fe, for lower Nd content, meanwhile the opposite trend is found when Ti content is 4 at.% (Fig. 4b). This allows us to conclude that there is a competitive
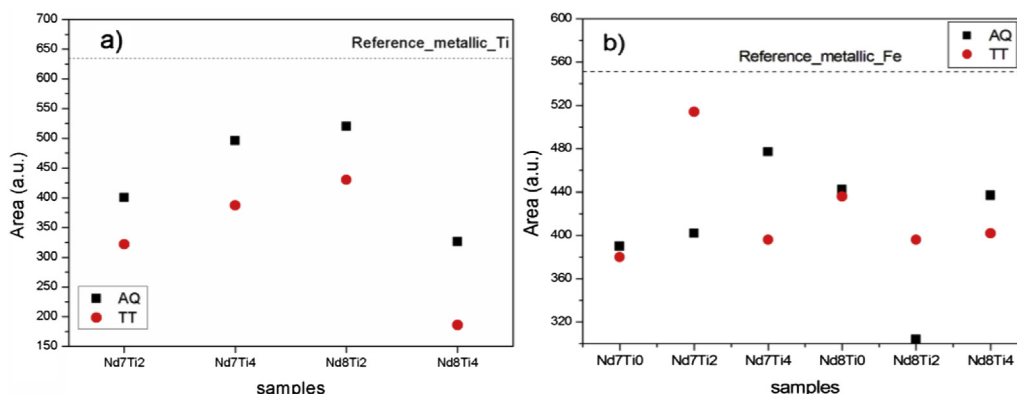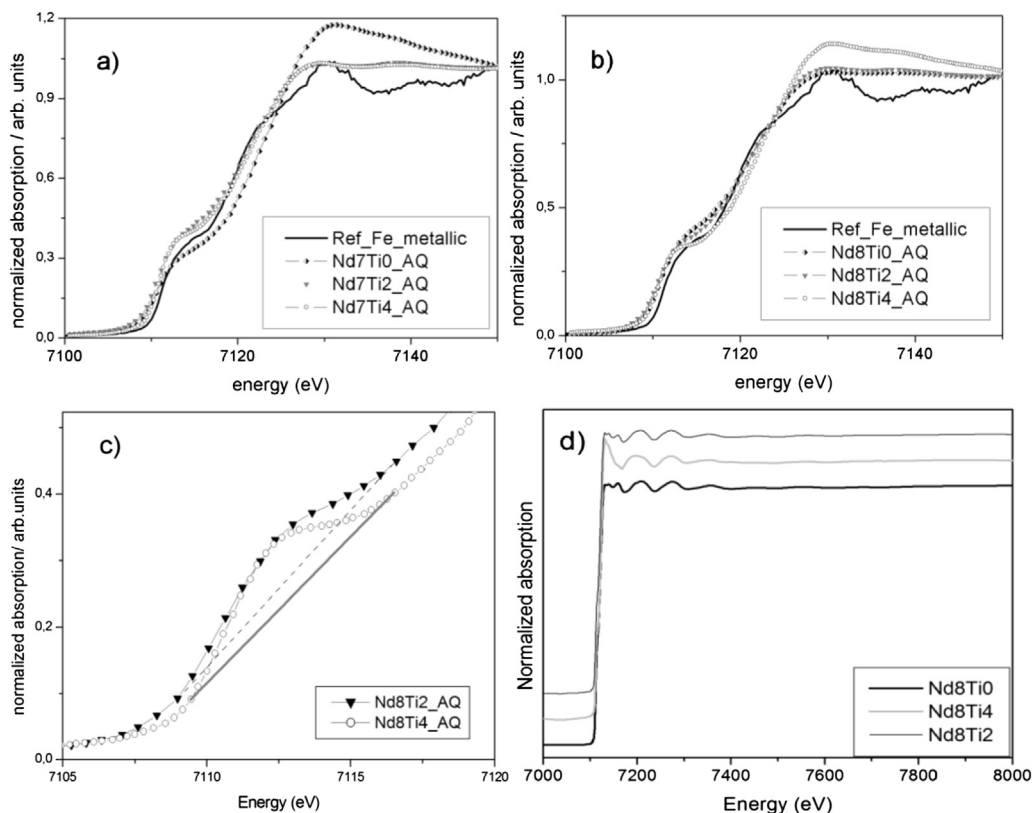

Fig. 2. Pre-edge area calculations (corresponding to 3d empty density states) of AQ and TT alloys as well as corresponding metallic reference at K-edge of a) Ti and b) Fe.

Fig. 3. Fe K-edge XANES signal of metallic Fe and AQ alloys for different Ti content (0,2,4 at.%): a) $y = 7$ at.% and b) $y = 8$ at.%. c) a zoom of pre-edge complex structure of Nd8Ti2_AQ and Nd8Ti4_AQ spectra. d) Normalized spectra of the AQ samples with $y = 8$ at.% showed in the complete range (the spectra are shifted along y axes for better visualization).

bonding of Ti and Nd with Fe atoms. It is worth mentioning that as in the case of Ti K-edge spectra, slight energy shifts at the Fe K-edge main line position toward higher values indicate partial oxidation of Fe.

### 3.3. As-quenched samples (AQ) vs. thermal treated (TT)

3.3.1. Ti K-edge XANES

Fig. 5 shows the annealing effect on the ribbons, as it can be concluded from the information based on the measurements at Ti K-edge. For all samples, we found that the 3d EDS of titanium is reduced after annealing (Fig. 2a), indicating that thermal annealing promotes filling of the Ti 3d states.

3.3.2. Fe K-edge XANES

From the comparison of EDS of iron's 3d states (Fig. 2b) of AQ and TT samples, we can highlight the following features. For samples without Ti, there are, practically, no differences in the EDS of 3d states of iron for AQ and TT samples. In samples containing 2 at.% of the additive, thermal treatment promotes higher 3d EDS of Fe. Meanwhile, in 4 at.% titanium-containing samples the trend is opposite (Fig. 6).

From the analysis of pre-edge structure area (both Ti and Fe K-edge), we can distinguish the following trends for all studied samples regarding their corresponding metallic reference: the 3d EDSs of Ti and Fe diminish as compared with the corresponding ones in XANES spectra of pure element references. In other words, the occupancy of 3d states of Fe and Ti in the samples is higher than
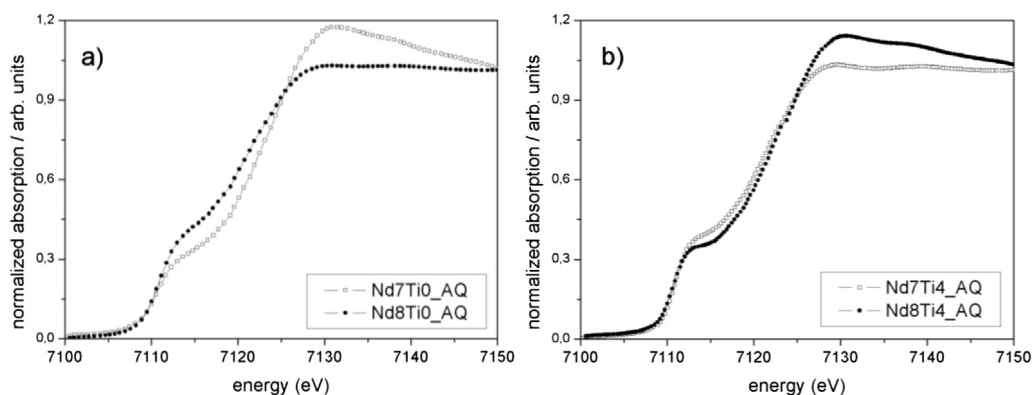
Fig. 4. Fe K-edge XANES signal of AQ alloys with varied Nd content for a) without Ti and b) 4 at.% of Ti.
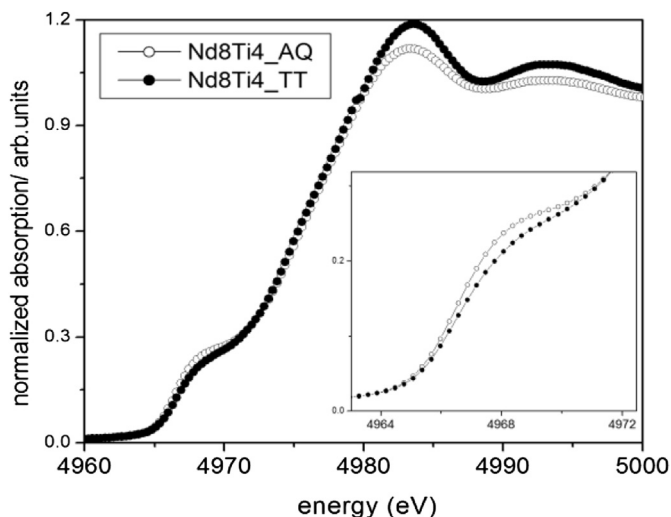
Fig. 5. Ti K-edge spectra of AQ and TT sample with $x = 4$ at.%, $y = 8$ at.%.

in the corresponding metallic references. This suggests that Fe and Ti behave like acceptors of electrons in their $3d$ bands when they are alloyed to the other elements in the Nd−Fe−B−Ti system.

3.4. Structure at short- and long-range

In Fig. 7 we show Fourier transformations of the oscillating part of the absorbing spectra of the TT samples containing 8 at.% of Nd, besides BCC-Fe FT taking as a reference. The main peak observed for all the FTs present here (Fig. 7), corresponds to Fe−Fe coordination (first near neighbors for the absorbing atom). The amplitude of the peak is directly related to the number of scattering atoms (first near neighbors) surrounding the absorbing atom (Fe) [19] and to the Debye−Waller factor (static and dynamic disorder). For instance, in the case of BCC-Fe, they are 8 Fe atoms 2.49 Å-distanced and 6 Fe atoms 2.87 Å-distanced from the central atom [20]. Taking into account these contributions, we performed a fitting procedure of BCC-Fe reference sample in the corresponding part of the spectrum (Fe−Fe coordination). As a result of the fit, a σ^2 parameter, associated with the Debye−Waller factor, is about 0.004. As the measure was carried out at only 15 K, we attribute the value of the Debye−Waller factor to, mainly, static (structural) disorder.
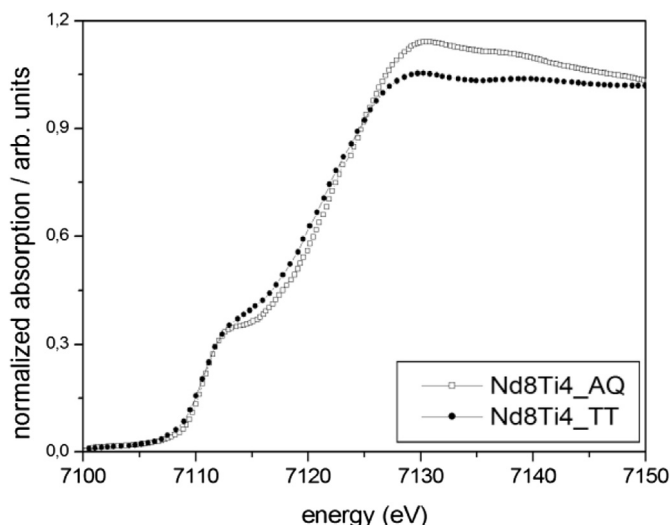

Fig. 6. Fe K-edge spectra of AQ and TT sample with $x = 4$ at.%, $y = 8$ at.%.

The FT of the sample with Nd reveals a clear diminishing of the main peak intensity. We attribute this fact to a larger static disorder around Fe atom probe. In the following text we explain how we have reached to such conclusion. We performed XRD measurement of the samples and the quantitative analysis (extracted from Rietveld analysis) of the composition of crystalline phases found in the samples is shown in Table 1. For instance, Nd8Ti0 sample besides the BCC-Fe phase (48%), has also the $Nd_2Fe_{14}B$ (30%), $Nd_2Fe_{23}B_3$ (12.5%) and minority $Nd_{1.1}Fe_4B_4$ phase. In all these structures, the Fe−Fe distances are very similar (about 2.5 Å) [20]. On the base of this, it is very complicated to fit the first peak of the FT for the ternary compound. Nevertheless, the Nd8Ti4 sample has a majority phase ($Nd_2Fe_{14}B$). This facilitates the FT analysis. Fe−Fe coordination was proposed during the fit of the main peak (they are 8 Fe atoms located at an averaged 2.54 Å). This is in accordance with the mean distance among Fe atoms in the structure of $Nd_2Fe_{14}B$ (Space Group 136, $P_{42/mnm}$) [20]. For the left shoulder, Fe−B coordination was proposed (present in $Fe_{23}B_6$ phase, found by XRD, at about 2.1 Å). Using the mentioned model, the best fitted FT of the Nd8Ti4 was achieved (Fig. 7b). The σ^2 parameter for the Fe−Fe coordination resulted to be considerably higher (0.007) than in the case of the BCC-Fe. This increase in the Debye−Waller factor and the fact both in BCC-Fe and $Nd_2Fe_{14}B$ the first near neighbors are 8 Fe atoms located almost at the same distances, clearly implies that the reduction of the main peak intensity in the FT mainly comes from a static disorder.

In previous studies of this system reported by two co-authors of this work [21], the XANES spectra at Nd L_3-edge ($2p \rightarrow 5d$ dipolar transitions) showed a difference in the white line intensities (depending on Nd and Ti content) indicating variation in available $5d$ states. It is important to remind that the electronic structure of Nd^0 of the latest shells is $5s^25p^66s^2$. In other words, the $5d$ state in such an atom is empty, without electrons. So far, the variation in EDSs of the Nd $5d$ states during the promotion of the electronic transitions after the atom ionization in the alloys unambiguously indicates some degree of occupancy of the $5d$ states before ionization in ground state. This demonstrates that Nd atoms (as well as Fe and Ti atoms) in the alloys are acceptors of electrons.

Thus we have obtained the evidence of acceptor behavior of Nd, Fe and Ti atoms. It suggests that boron is playing the role of electron-donor. It is not a trivial conclusion because this element, as it is well known, is usually employed as electron-acceptor in the semiconducting industry [22]. Studying a metallic glass system Ni−B, Luo et al. showed that boron is an electron-donor in amorphous alloy, while nickel is an electron-acceptor [23]. Their results are consistent with ours in this case. Boron is one of all four elements (present in the alloys) that has its outer shell occupied with only one electron ($2p^1$) that could be donated with more facility. This is the simplest scenario of direct charge transfer which could occur in the system. Nevertheless, we cannot discard other, more complex mechanisms, of indirect charge transfer among all or some of these elements. A supporting reason for this conclusion is the observed tendency for the EDS of Nd $5d$ and Fe $3d$ states reported previously [21] when the average EDS increased in Nd and decreased in Fe and vice versa, depending on the Ti concentration.

XAS and XPS are techniques that provide information about electronic structure of material. Even though they bring information from different regions of sample when they are in use, together they complement each other helping to get a better understanding of the material under investigation.

3.5. XPS

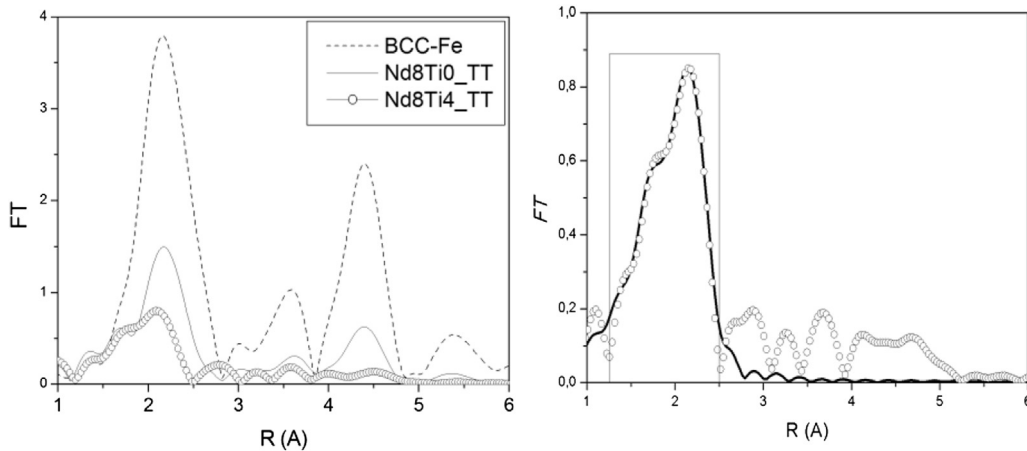Photoelectron spectroscopy was used to elucidate the chemical nature and surface exposure of the ribbons.

Fig. 7. FT of $k^3\chi(k)$ in the interval 2–14 Å^{-1} of TT samples with 8 at.% of neodymium ($x = 0$ and 4 at.%). BCC-Fe is shown as a reference signal (left); the fit (solid line) of the first shell of Fe in Nd8Ti4_TT sample (right).

3.5.1. Survey

In Fig. 8, a typical XPS survey spectrum corresponding to Nd7Ti4_TT sample and taken in 0–1200 eV binding energy (BE) range, is shown. The BEs are related to the Fermi level ($E_F = 0$ eV). We have identified the peaks (including both photoemission and Auger ones) using a standard database of the CasaXPS software. As it can be seen, besides of the expected alloy elements, oxygen and carbon atoms were found on the surfaces. It is not surprising because like any surface, the surface of the ribbons reacts with its environment.

Comparing photoemission spectra of AQ and TT alloys, it can be seen that Nd/Fe area ratio is higher for the annealed ones indicating an Nd enriched surface after the crystallization procedure (Fig. 9). This is consistent with reports on Nd-rich zones on the external part of the NdFeB magnets after heat treatment [24]. We also note from the positions of Nd $3d_{5/2}$ (*FWHM* ≈ 3.0 eV) and $3d_{3/2}$ (*FWHM* ≈ 4.0 eV) photoelectrons' BE that some neodymium atoms at the surface are in metallic condition, Nd^0 ($3d_{3/2}$ photoelectron: ≈ 978 eV), while another fraction of this chemical element (with higher binding energies) corresponds to Nd^{3+} ($3d_{3/2}$ photoelectron: ≈ 982–983 eV) (Fig. 10a), in agreement with [25]. When neodymium interacts with oxygen, valence electrons are transferred from the metal to oxygen with a variation of the electrical screening of inner shells. As a result, the binding energies of the inner electrons of the metal ion are increasing. It is well known that Nd is a highly oxidizing element [8,24].

Similar information is obtained from the analysis of the BE of Fe photoelectrons. Fe $2p_{3/2}$ with 707 eV and $2p_{1/2}$ with 720 eV photoemission peaks are detected as expected for metallic Fe [26], while the peaks shifted to higher BE (the peak $2p_{3/2}$ with nearly 711 eV and the peak $2p_{1/2}$ with nearly 724 eV) correspond to Fe^{3+} (Fig. 10b) in agreement with [27]. This is consistent with earlier

Table 1
Crystalline phases identified by XRD in TT samples (in atomic weight percentage (% wt.)).

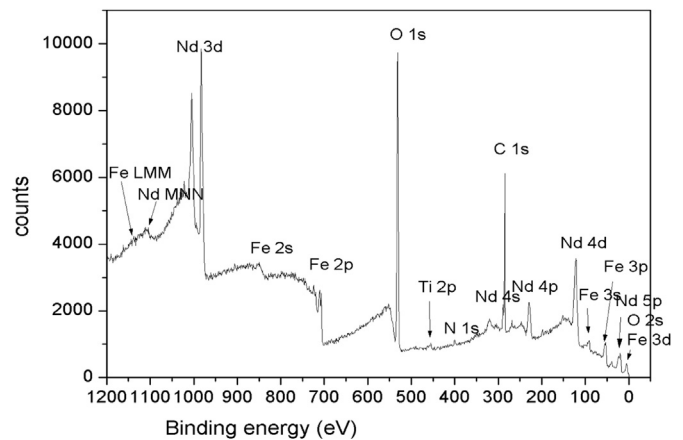| Sample	Nd$_2$Fe$_{14}$B	Nd$_2$Fe$_{23}$B$_3$	BCC-iron	Fe$_{23}$B$_6$	TiB$_2$	Other phases (<10%)
Nd7Ti0	11.5	19.5	62.4	–	–	Nd$_{1.1}$Fe$_4$B$_4$
Nd8Ti0	30.0	12.5	48.1	–	–	Nd$_{1.1}$Fe$_4$B$_4$
Nd7Ti2	35.2	48.5	–	<3	13.7	Fe$_2$B
Nd7Ti4	49.8	<3	–	41.8	7.8	Fe$_2$B
Nd8Ti2	77.5	<3	–	11.7	6.9	Fe$_2$B
Nd8Ti4	82.9	<3	–	4.8	10.3	Fe$_2$B

Fig. 8. XPS survey scan of Nd7Ti4_TT alloy.
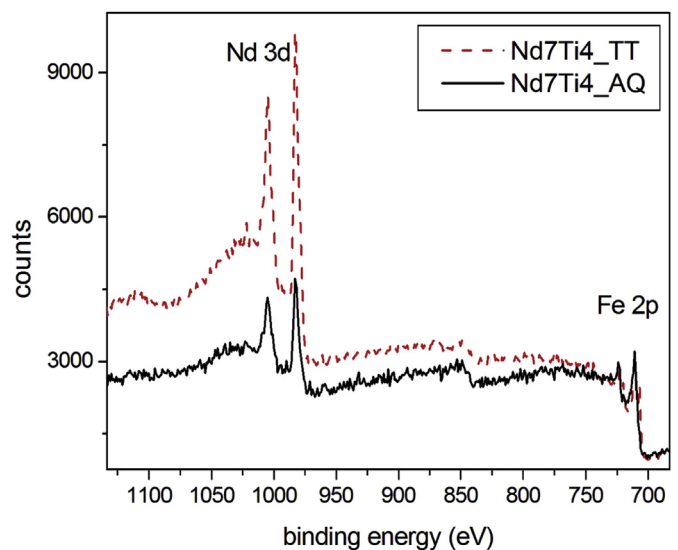
Fig. 9. XPS survey of AQ and TT ribbons with $y = 7$ at.%, $x = 4$ at.% (a zoom of the specific region).
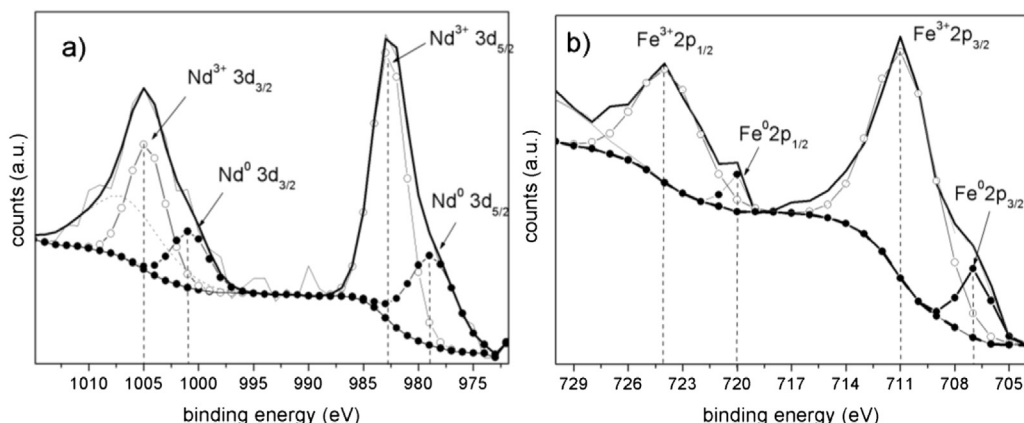
Fig. 10. XPS of AQ samples: a) 3d Nd peaks of Nd7Ti4; b) 2p Fe peaks of Nd7Ti2. The resolution is 1 eV.

report by Li et al. [8] who found neodymium and iron oxides phases after submitting NdFeB to heat treatment under high temperature.

We emphasize that even though the survey spectra were collected with 1 eV step (which is somewhat large for precise fitting), nevertheless their analysis leads to qualitatively correct information.

3.5.2. Ti 2p

In order to give insight on the additive element, we measured short-range bind energy region (450–470 eV) with more spectral resolution. Fig. 11 shows typical Ti 2p core-level spectrum of TT ribbon with $y = 8$ at.% and $x = 4$ at.%. The spectrum displays the spin-orbit splitting characteristic of Ti 2p levels. The intensity ratio of the Ti 2$p_{3/2}$ and Ti 2$p_{1/2}$ peaks is constrained to be 2:1 during the fitting procedure. The width of the Ti 2$p_{1/2}$ peak is broadened as compared to the Ti 2$p_{3/2}$ one due to Coster–Kronig effect [28]. To clarify the peak widths, doublet splitting ($\Delta = 6.05$ eV for Ti(0), $\Delta = 5.7$ eV for Ti(IV)) and shapes (asymmetric for the metallic component) were used [29]. Shirley background was used during the fitting procedure.

It was found that we are encountered with two different Ti 2p electrons (from BE values) for all the ribbon surfaces. As it can be

seen from Fig. 11 and Table 2 (BE values extracted from the fitting procedure), Ti atom on the surface is in both metallic (Ti^0) and oxidized state (Ti^{4+}) [29,30].

We did not find any significant shift in BEs for Ti^{4+} 2$p_{3/2}$ electrons as a function of Ti concentration ($\approx 458.4 \pm 0.1$ eV) and/or synthesis conditions. TiO$_2$ structure is the most probable phase to be formed with Ti^{4+} oxidation state (a more stable titanium oxide form). The BE values are found to be in the 453.25–454.13 eV region relative to metallic Ti 2$p_{3/2}$ electrons. As it can be seen from Table 2, the *FWHM* values of TT samples extracted from the fitting procedure, are slightly enhanced as compared with the ones of AQ samples. We suggest that it can be attributed to a convolution of two peaks of Ti in metallic state. One of them is, undoubtedly, Ti in TiB$_2$ compound [31] which was detected in TT samples by XRD (Table 2). The second one could be due to a presence of other Ti metallic bond, for instance, Ti atoms replacing iron atoms in one (or more) phase present in the samples as it was suggested in Ref. [21]. This is the most probable scenario for ribbons after thermal treatment. We note that annealed samples have a greater number of metallic Ti atoms as compared with as-quenched ones.

The presence of oxidized titanium at the surface, as it was determined by XPS, complements the previously discussed data obtained by XAS. As it can be seen from figures containing XANES spectra of the ribbons, the spectra are shifted with respect to the reference signal (metallic foil). This is an indication of partial oxidation of titanium.

4. Conclusions

The electronic structure of Nd$_y$Fe$_{(86-y-x)}$B$_{14}$Ti$_x$ ($x = 0,2,4$; $y = 7,8$ at.%) ribbons was studied. Using XANES, it was found that Ti doping influences the structure of Fe sub-band for both as-quenched and thermally treated ribbons. In Nd–Fe–B–Ti alloys, Ti and Fe atoms behave as electron acceptors in the 3d levels.

Fig. 11. XPS of Ti 2p electrons of AQ sample with $y = 8$ at.%, $x = 4$ at.%. The bold line is a fit one.

Table 2
The parameters obtained from XPS analysis. A^0/A^{4+} is a ratio of spectral areas corresponding to metallic and oxidized states.

Sample	Ti^0 2$p_{3/2}$ (eV)	FWHM (eV)	Ti^{+4} 2$p_{3/2}$ (eV)	FWHM (eV)	A^0/A^{4+}
Nd7Ti2_AQ	453.26	0.70	458.45	1.84	0.08
Nd7Ti4_AQ	453.25	0.95	458.36	1.66	0.20
Nd8Ti2_AQ	453.91	0.72	458.36	1.72	0.11
Nd8Ti4_AQ	453.99	0.96	458.50	1.86	0.21
Nd7Ti2_TT	454.05	1.50	458.40	1.75	0.44
Nd7Ti4_TT	454.13	1.22	458.41	2.02	1.20
Nd8Ti2_TT	454.09	1.31	458.42	1.99	0.79

Thermal treatment influences occupancy of the 3*d* states in both transition metals. By XPS, Nd, Fe and Ti atoms on the surface are found in both metallic and oxidized state. Annealing procedure decreases the number of oxidized titanium states favoring the appearance of titanium with metallic-type bonds on ribbons surface.

References

[1] J.L. Li, L.J. Zhang, Y.X. Wang, L.P. Wang, H. Li, B.J. Ye, Q.J. Xue, Effect and mechanism of ion bombardment on coercive force of NdFeB magnet, Mater. Lett. 98 (2013) 102–104.

[2] Y. Matsuura, J. Hoshijima, R. Ishii, Relation between $Nd_2Fe_{14}B$ grain alignment and coercive force decrease ratio in NdFeB sintered magnets, J. Magn. Magn. Mater. 336 (2013) 88–92.

[3] B.B. Straumal, Yu. O. Kucheev, I.L. Yatskovskaya, I.V. Mogilnikova, G. Schütz, A.N. Nekrasov, B. Baretzky, Grain boundary wetting in the NdFeB-based hard magnetic alloys, J. Mater. Sci. 47 (24) (2012) 8352–8359.

[4] M. Leonowicz, M. Spyra, E. Jezierska, Improvement of the properties of hard magnetic NdFeb/Fe nanocomposites by minor addition of refractory metals, Mech. Adv. Mater. Struct. 18 (3) (2011) 181–184.

[5] V. Bilovol, S. Ferrari, L.G. Pampillo, D. Derewnicka, M. Spyra, F.D. Saccone, Influence of Nb doping on magnetic properties of nanocrystalline Nd–Fe–B alloys, IEEE Trans. Magn. 49 (No. 8) (August 2013) 4622–4625.

[6] Marzena Spyra, Daniela Derewnicka, Marcin Leonowicz, Lean neodymium Nd–Fe–B magnets containing minor addition of titanium, Phys. Status Solidi A 207 (5) (2010) 1170–1173.

[7] Marcin Leonowicz, Marzena Spyra, Elżbieta Jezierska, Hard magnetic, low neodymium NdFeB MeltSpun alloys containing refractory metals, AIP Conf. Proc. 1347 (2011) 103.

[8] Y. Li, H.E. Evans, I.R. Harris, I.P. Jones, The oxidation of NdFeB magnets, Oxid. Metals 59 (Nos. 1/2) (February 2003).

[9] L. Yang, L. Zhen, C.Y. Xu, X.Y. Sun, W.Z. Shao, Effects of proton irradiation on electronic structure of NdFeB permanent magnets, Nucl. Instrum. Methods Phys. Res. B 267 (2009) 3084–3086.

[10] Minna Haavisto, Sampo Tuominen, Harri Kankaanpää, Martti Paju, Time dependence of demagnetization and flux losses occurring in sintered Nd–Fe–B permanent magnets, IEEE Trans. Magn. 46 (NO. 9) (2010).

[11] Ran Zhang, Ying Liu, Jun Li, Shengji Gao, Mingjing Tu, Effect of Ti&C substitution on the magnetic properties an microstructures of rapidly-quenched NdFeB alloy, Mater. Charact. 59 (2008) 642–646.

[12] Hideya Onodera, Hiroshi Yamauchi, Motohiko Yamada, Hisao Yamamoto, Mössbaur study of the intermetallic compound $Nd_2Fe_{14}B$. II. Temperature dependence and spin reorientation, J. Magn. Magn. Mater. 68 (1987) 15–27.

[13] L. Yang, L. Zhen, C.Y. Xu, X.Y. Sun, W.Z. Shao, Effects of proton irradiation on structure of NdFeB permanent magnets studied by X-ray diffraction and X-ray absorption fine structure, J. Magn. Magn. Mater. 323 (2011) 4–6.

[14] L. Lutterotti, S. Matthies, H.-R. Wenk, A.J. Schultz, J. Richardson, Texture and structure analysis of deformed limestone from neutron diffraction spectra, J. Appl. Phys. 81 (2) (1997) 594–600.

[15] J.E. Müller, O. Jepsen, J.W. Wilkins, X-ray absorption spectra: K-edges of 3d transition metals, L-edges of 3d and 4d metals, and M-edges of palladium, Solid State Commun. 5 (No.5) (1982) 365–368.

[16] F. de Groot, G. Vankó, P. Glatzel, The 1s X-ray absorption pre-edge structures in transition metal oxides, J. Phys. Condens. Matter 21 (2009) 104207.

[17] G.L. Glen, C.G. Dodd, Use of molecular orbital theory to interpret X-ray K-absorption spectral data, J. Appl. Phys. 39 (1968) 5372.

[18] L.A. Grunes, Study of the K-edges of 3d transition metals in pure and oxide form by X-ray-absorption spectroscopy, Phys. Rev. B 27 (No. 4) (1983) 2111–2131.

[19] E.A. Stern, D.E. Sayers, F.W. Lytle, Extended X-ray-absorption fine-structure technique. III. Determination of physical parameters, Phys. Rev. B 11 (1975) 4836–4846.

[20] Crystallography Open Database, http://www.crystallography.net.

[21] D. Derewnicka, E. Lede, M.R. Pagnola, F.D. Saccone, M. Spyra, M. Leonowicz, L.G. Pampillo, Transformation of the crystalline and electron structures of NdFeB alloys modified with Titanium, in: Proceedings of the 22nd International Workshop on Rare Earth Magnets and their Applications, 2012, pp. 313–316. Nagasaki, Japan.

[22] Mariko Suzuki, Hiroaki Yoshida, Naoshi Sakuma, Tomio Ono, Tadashi Sakai, Masahiko Ogura, Hideyo Okushi, Satoshi Koizumi, Electrical properties of B-related acceptor in B-doped homoepitaxial diamond layers grown by microwave plasma CVD, Diam. Relat. Mater. 13 (1) (January 2004) 198–202.

[23] C. Luo, B.-R. Shen, K.-N. Fan, J.-F. Deng, H.-L. Liu, Theoretical study on the local structure and properties of electron transfer of Ni–B amorphous alloy, Acta Chim. Sin. 58 (8) (2000) 948–952.

[24] S. Oswald, S. Fähler, S. Baunack, XPS and AES investigations of hard magnetic Nd–Fe–B films, Appl. Surf. Sci. 252 (2005) 218–222.

[25] V.N. Rai, B.N. Raja Sekhar, P. Tiwari, R.J. Kshirsagar, S.K. Deb, Spectroscopic studies of gamma irradiated Nd doped phosphate glasses, J. Non-crystalline Solids 357 (22–23) (15 November 2011) 3757–3764.

[26] Xingyu Gao, Swee Ching Tan, A.T.S. Wee, Junhua Wu, Lingbing Kong, Xiaojiang Yu, H.O. Moser, Structural and magnetic characterization of soft-magnetic FeCo alloy nanoparticles, J. Electron Spectrosc. Relat. Phenom. 150 (2006) 11–14.

[27] Toru Yamashita, Peter Hayes, Analysis of XPS spectra of Fe^{2+} and Fe^{3+} ions in oxide materials, Appl. Surf. Sci. 254 (2008) 2441–2449.

[28] G. Silversmit, D. Depla, H. Poelman, G.B. Marin, R. De Gryse, An XPS study on the surface reduction of $V_2O_5(0\ 0\ 1)$ induced by Ar^+ ion bombardment, Surf. Sci. 600 (2006) 3512.

[29] Mark C. Biesinger, Leo W.M. Lau, Andrea R. Gerson, Roger St.C. Smart, Resolving surface chemical states in XPS analysis of first row transition metals, oxides and hydroxides: Sc, Ti, V, Cu and Zn, Appl. Surf. Sci. 257 (2010) 887–898.

[30] Huogen Huang, Tianwei Liu, Zhi Zhang, Xiaoqiu Ye, Lizhu Luo, Xiangdong Zhang, Deuterium storage of $Ti_{40}Zr_{40}Ni_{20}$ icosahedral quasicrystal, Int. J. Hydrogen Energy 37 (2012) 15204–15209.

[31] K. Chu, Y.H. Lu, Y.G. Shen, Structural and mechanical properties of titanium and titanium diboride monolayers and Ti/TiB2 multilayers, Thin Solid Films 516 (2008) 5313–5317.